Journal of Energy

VOLUME 61 Number 1–4 | 2012 Special Issue

journal homepage: http://journalofenergy.com/

Ralf Wittmaack
Siemens E T TR EU PN EN4
Ralf.Wittmaack@Siemens.com

CFD SIMULATIONS OF OIL IMMERSED AND DRY TYPE TRANSFORMERS

SUMMARY

At Siemens the in-house CFD code UniFlow is employed to investigate fluid flow and heat transfer in oil immersed and dry type transformers as well as transformer components like windings, cores, tank walls, and radiators. We outline its physical models and numerical solution methods.

As an oil transformer application of the method, the simulation of oil flow and heat transfer in 5 windings of a prototype transformer with ONAN/ONAF cooling mode is described. It corresponds to a heat run test with the total losses.

Furthermore, we outline an application to an AFWF cast resin transformer prototype operated at ships in an enclosure. The ventilator driven air flow is cooled by sea water. In addition to the LV and HV windings the core is simulated. Here also the heat radiation makes a significant contribution to the heat transfer.

Key words: Thermal design, CFD, physical models, radiant heat transfer, numerical methods

1. INTRODUCTION

Thanks to its flexibility and accuracy CFD (Computational Fluid Dynamics) is becoming more and more frequently applied to analyses of transformer thermal design. This follows the trend established in other branches of advanced technology development, like aerospace, automotive, and power generation, where CFD simulations since many years are indispensable parts of the product development cycles.

Employing commercial CFD codes, several detailed studies of disc-type transformer windings were performed, e.g., by Torriano, Chaaban, and Picher [1]. Moreover, extended full geometry CFD analyses coupled to electromagnetic simulation of the load and no-load losses in core and windings were presented, e.g., by Smolka and Nowak [2].

Our intention is to provide a simulation method that may be used for detailed CFD analyses on fine grids as well as for simplified coarse grid studies. The in-house code UniFlow is designed to be easily applicable also by users that have only little experience in CFD. For this reason, e.g., in simple geometries it allows to set-up complex flow and heat transfer calculations without prior grid generation with an auxiliary code and coupling of the fluid and solid regions.

R. Wittmaack, CFD simulations of oil immersed and dry type transformers, Journal of Energy, vol. 61 Number 1–4 (2012) Special Issue, p. 129-138
https://doi.org/10.37798/2012611-4245

2. PHYSICAL MODELS AND NUMERICAL METHODS

2.1. Physical models

Our physical model is aimed at investigating flows with several kinds of heat transfer in complex geometry. It simulates the flow of single-component incompressible Newtonian fluids in a three-dimensional geometry. In addition to the fluids, in gaseous or liquid state, several structural materials are considered as hydrodynamic obstacles and thermodynamic heat structures. The hydrodynamics is described by the continuity and the Navier-Stokes equation. For the simulation of turbulence the algebraic Baldwin-Lomax eddy viscosity model is available. To simulate the transition between laminar and turbulent flows the algebraic transition models of Drela and Mayle are employed.

For temperature dependent density or material properties of the viscous stress tensor, the hydrodynamics of the fluid is coupled to the thermodynamics. For this reason, internal heat transfer (by convection and conduction) and heat generation by internal sources as well as heat transfer to the surroundings are modelled via a heat transport equation. To allow for simulation of phase transitions it is provided in enthalpy formulation. At the rigid boundaries heat conduction is considered. For coarse grids convective heat transfer coefficients may be employed at solid-liquid interfaces. Radiant heat transfer is simulated at structural material surfaces. The material properties (density, dynamic viscosity, specific heat, heat conductivity, and convective heat transfer coefficient) depend on the temperature.

2.1.1. Dynamic equations

Our dynamic equations are written in Cartesian coordinates. The continuity equation for incompressible flow is [3]

$$\frac{\partial}{\partial x^m}\left(\rho\ v^m\right)=0\,, \tag{1}$$

where: ρ is density and v velocity. x are the space coordinates and we use Einstein's summation convention for the space direction index m. Introduction of the continuity equation into the Navier-Stokes equation [3] leads to a momentum equation in strong conservation form,

$$\rho\frac{\partial v_i}{\partial t}+\frac{\partial}{\partial x^m}\left[\rho\ v_i\ v^m-\mu\ \left(\frac{\partial v_i}{\partial x_m}+\frac{\partial v^m}{\partial x^i}\right)\right]=-\frac{\partial p}{\partial x^i}+\rho\ g_i\,, \tag{2}$$

where: t is time, p pressure, and g gravitational acceleration. After inclusion of the continuity equation our heat transport equation in strong conservation form reads

$$\rho\frac{\partial h}{\partial t}+\frac{\partial}{\partial x^m}\left(\rho\ h\ v^m-\lambda\ \frac{\partial T}{\partial x_m}\right)=P_d\,. \tag{3}$$

Here h is specific enthalpy, T temperature, λ heat conductivity, and P_d density of the heat sources or sinks.

2.1.2. Radiant heat transfer model

Radiant heat transfer may be simulated between structural material surfaces adjacent to the fluid. The employed radiation model assumes that the radiating surfaces are boundaries of a hollow space with linear dimension much greater than their distance. It is applicable for, e.g., parallel plates and concentric cylinders. With this simplifying assumption the power received by surface 'a' via the heat transfer from surface 'b' to surface 'a' is [4]

$$P_{ab}=c_{ab}\ A_{ab}\ \left(\ T_b^{\,4}-T_a^{\,4}\right);\ \ c_{ab}:=\frac{\sigma}{\frac{1}{\varepsilon_a}+\frac{A_a}{A_b}\left(\frac{1}{\varepsilon_b}\ -\ 1\right)}\,. \tag{4}$$

Here A is area of a radiating structural material surface, T surface temperature, $\sigma = 5.67051 \cdot 10^{-8} \frac{W}{m^2 K^4}$ the Stefan-Boltzmann constant, and ε emissivity of a structural material surface. Computation domain nodes undergoing radiant heat transfer may have their radiation partner nodes inside the computation domain or at the boundary.

2.2. Numerical methods

For the numerical representation of our model we developed a finite volume method and employ boundary fitted, curvilinear, non-orthogonal, block-structured grids. The blocks may be connected via 1-to-1 or patched couplings. The arrangement of the dynamic variables in the control volumes of the grid is collocated at the node centre. The dynamic equations are solved sequentially. For the solution of the momentum, pressure-correction, and heat transport equations we use implicit schemes. The system of continuity and momentum equations is solved by a SIMPLE [5], SIMPLEC [6], or PISO [7] algorithm.

To speed-up the code execution and to ease the estimation of discretisation errors a FAS multi-grid algorithm is employed [8]. It is a geometric approach with standard coarsening applied to the outer iterations, visiting the grid levels in V-cycles. For steady-state problems it operates as full multi-grid algorithm (FMG) while for transient problems the algorithm starts at the finest grid.

For the efficient solution of sparse linear equations several algorithms are available. The parabolic momentum and heat transport equations may be solved with SIP solvers that are modified to handle block couplings via the residual vector [5]. For the elliptic pressure-correction equation an aggregation-based algebraic multi-grid algorithm [9] is available in addition.

3. APPLICATIONS

In the following 2 transformer applications of our method are outlined. In these geometrically simple simulations we analyse only the middle of the 3 limbs in 2-dimensional cylindrical coordinate systems with rectangular grids. x_1 designates the radial and x_3 the vertical space direction. Geometrically more complex UniFlow calculations are described, e.g., in [10].

In both of the applications mentioned in this paper we analyse the steady state. Furthermore, load losses are calculated by Maxwell-solvers and subsequently mapped to the CFD grids.

Another common feature of the presented applications is that only the active part is studied with prescribed fluid flow via in- and outlet boundary conditions, i.e., only parts of the entire coolant loops are considered.

3.1. Oil transformer prototype

As an oil transformer application we consider the windings of a prototype transformer operated in ONAN or ONAF cooling mode. The rated power is 63 MVA in the HV windings. At this transformer a set of windings at each limb consists of LV, MVR, MV, HV, and HVR windings. Our thermal simulation corresponds to a heat run test with the total losses, i.e., including the no-load losses of the core.

Figure 1 – Prototype transformer with ONAN / ONAF cooling in test field

3.1.1. Spatial discretisation and boundary layer thickness

A grid with 4 blocks is used for spatial discretisation. The 4 blocks represent the LV, MVR, MV, and HV / HVR windings respectively. Patched couplings are employed at the interfaces of the grid blocks. The grid is made up of 31023 nodes in the computation domain, where 14862 represent the oil while the remaining 16161 nodes correspond to the winding materials. The node lengths are 2 to 10 mm.

With the height of the windings as characteristic length l = 1.684 m and estimations of the oil velocity and temperature, the Reynolds number is R = 10880 and the Prandtl number is Pr = 61. This indicates laminar oil flow, where the hydrodynamic and thermal boundary layer thickness may be estimated via [3]

$$\delta_h \propto \frac{l}{\sqrt{R}} \quad ; \quad \delta_t \propto \delta_h \ \mathrm{Pr}^{-\frac{1}{3}} \tag{5}$$

This leads to a hydrodynamic boundary layer thickness of 16.1 mm and a thermal boundary layer thickness of 4.1 mm. As d_t is more than 2 times the node length at the interfaces to the structural materials, the grid provides a reasonable resolution of the boundary layers.

3.1.2. Material properties

In the windings we consider material mixtures to account for the influence of the insulation between the Cu wires on the material properties density ρ, specific heat at constant pressure c_p, and heat conductivity λ. The mixture properties are calculated via

$$\rho_{mix} := \sum_{i=1}^{n_{mat}} \alpha_i \ \rho_i \qquad \alpha_i := \frac{V_i}{V}$$

$$c_{p\,mix} := \sum_{i=1}^{n_{mat}} x_i \ c_{pi} \qquad x_i := \alpha_i \ \frac{\rho_i}{\rho_{mix}} \tag{6}$$

$$\lambda_{mix} := \left(\sum_{i=1}^{n_{mat}} \frac{\alpha_i}{\lambda_i} \right)^{-1}$$

where: α is volume fraction, x mass fraction, V volume, and n_{mat} no. of material constituents. Compared to pure Cu, the most relevant effect of mixture properties is a significant reduction of the heat conductivity.

3.1.3. Power density of load losses

The next figure shows the spatial distribution of the load losses calculated by the Maxwell-solver SAPR and its subsequent mapping to the CFD grid.

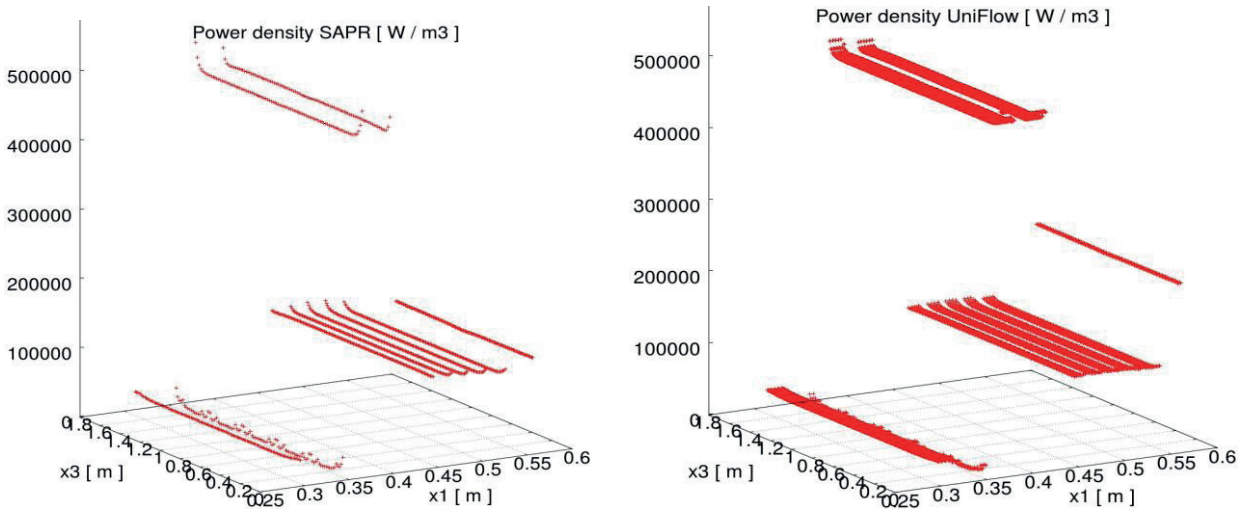

Figure 2 – Power density of load losses in ONAF transformer windings

As the CFD model includes only the inner half of the HVR windings the mapped power density is twice as high here. For this reason, in the UniFlow run in the HVR only half the power density shown in the figure is used.

3.1.4. Boundary conditions

As only a part of the oil natural convection loop is simulated, the inlet mass flows and temperatures are taken from integral thermo-hydraulic calculations. Adiabatic conditions are assumed at all computation domain boundaries, except the in- and outlets. For this reason only the inner half of the HVR windings is considered.

3.1.5. Simulation results

The next figure shows a vector representation of the velocity and its vertical component in the ONAF run. At the right figure the different colours are related to data of different grid blocks. As a result of its high power density of the load losses, the highest velocities occur in the MV windings. For ONAN cooling the oil velocity is similar but slightly smaller than for ONAF.

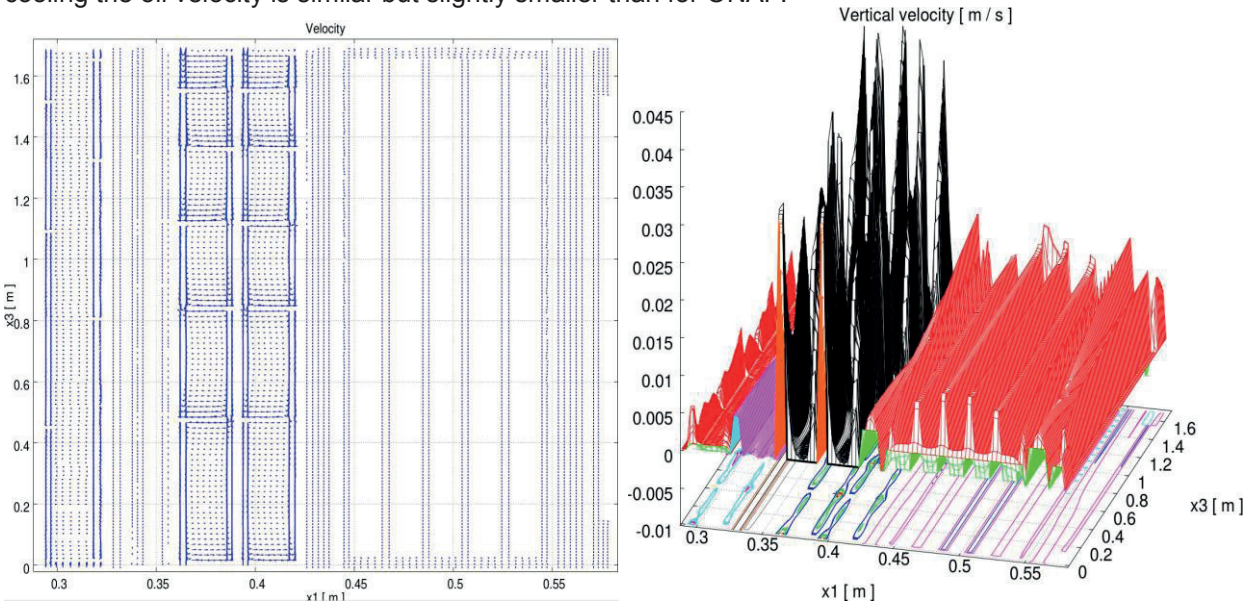

Figure 3 – Oil velocity and vertical velocity component in ONAF simulation

The next figure shows that the temperature distributions of oil and windings in the ONAN and ONAF simulations are similar, but the ONAF values are higher. The winding temperatures are closely related to the local oil velocity and the power density. Due to its high power density of the load losses, the highest temperatures are encountered in the MV windings. The adiabatic boundary condition on top and at the bottom of the MV windings causes enhanced temperatures at these locations.

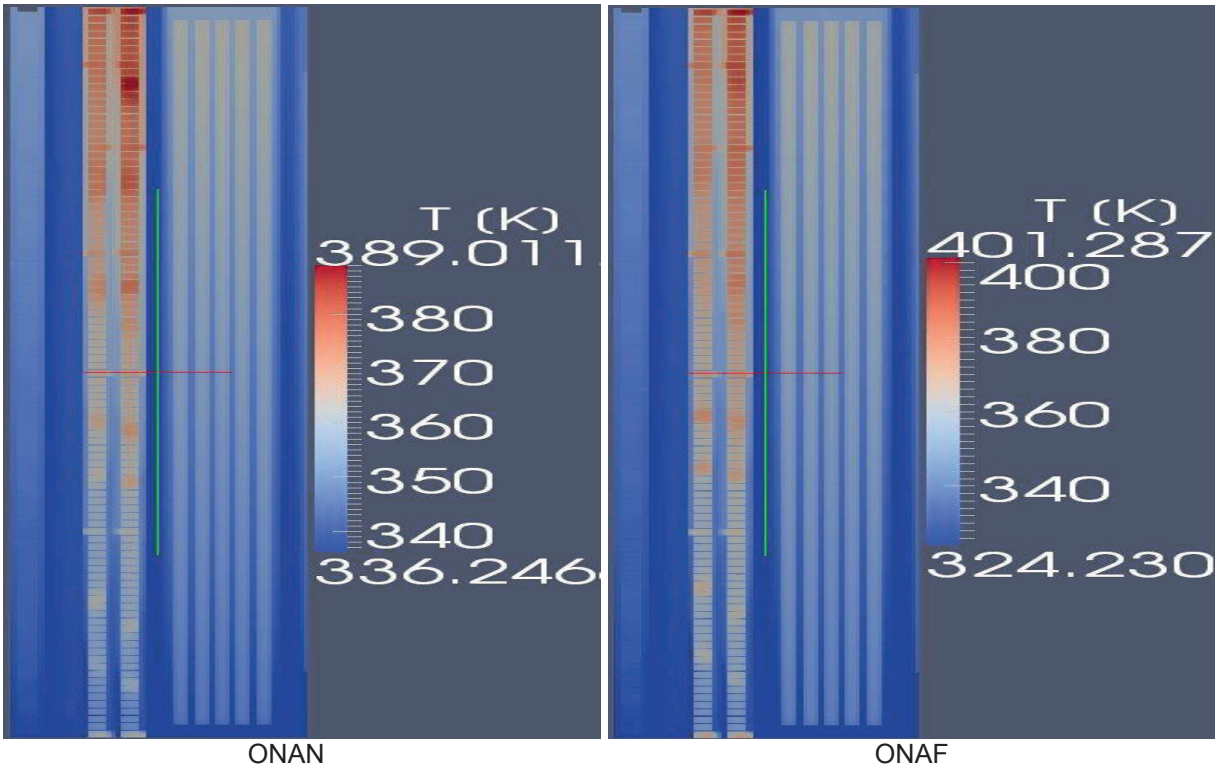

ONAN ONAF

Figure 4 – Temperatures in ONAN and ONAF simulations

The investigated conditions in our analysis do not lead to critical structural material temperatures in the transformer. On the other hand, the maximum oil temperature is close to values where cracking might take place and would be critical for its long-term stability.

3.2. Cast resin transformer for ships

As a cast resin transformer application we consider an AFWF transformer operated at ships in an enclosure. The ventilator driven air flow is cooled by sea water. A set of windings at each limb consists of three LV and one HV windings. We analyse the core and the windings with prescribed air flow via in- and outlet boundary conditions imposed by the ventilator.

Figure 5 – Side and top views of cast resin transformer without enclosure

The right side of the figure shows that between the LV and HV windings there is a thin polyester radiation cylinder. This enhances the heat transfer to the air.

3.2.1. Spatial discretisation and boundary layer thickness

A single-block grid with 38528 computation domain nodes is used for spatial discretisation. 27633 nodes represent the air while the remaining 10895 nodes correspond to structural materials. The node lengths are 1 to 54 mm.

With the height of the HV windings as characteristic length and estimations of the air velocity and temperature, the Reynolds number is R = 270000 and the Prandtl number Pr = 0.71. The vertical air flow along the windings resembles flow along a flat plate, where the transition from laminar to turbulent flow occurs between R = 3.5 * 10^5 and 10^6 [11]. This indicates that the air flow is laminar, i.e., the hydrodynamic and thermal boundary layer thickness may be estimated via (5). This leads to δ_h = 2 mm and δ_t = 2.2 mm at the upper end of the windings, i.e., the grid of our simulation of the cast resin transformer for ships is fine enough to resolve the hydrodynamic and thermal boundary layers.

3.2.2. Material properties

The structural materials considered in the simulation are steel of the core, Al of LV and HV windings, cast resin, prepreg, polyester, and Cr-Ni steel of the enclosure. The layers of the aluminium conductor and the prepreg / polyester insulation at the LV and HV windings are too thin to be resolved in the simulation. However, the vertical orientation of the layers leads to a heat conductivity of 237 W/(m K) in the vertical and 2.2 W/(m K) in the radial direction. To take this into account, we use prepreg / polyester insulation at the inner and outer boundaries of the LV and HV windings.

3.2.3. Power density of load and no-load losses

The next figure shows the spatial distribution of the load losses calculated by the in-house Maxwell-solver empower and its subsequent mapping to the CFD grid. It indicates a strong increase of the losses at the lower and upper end of the windings related to the radial component of the oscillating magnetic field. The high peak values correspond to the LV windings.

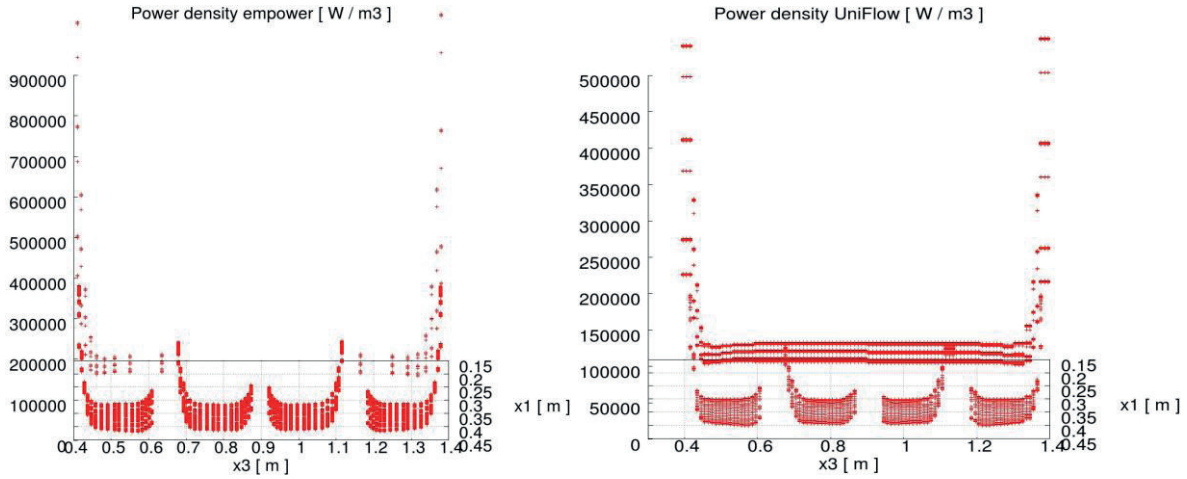

Figure 6 – Power density of load losses in cast resin transformer windings

The spatial distributions of the power density of the Maxwell-solver and CFD simulation are similar. The values mapped to the CFD grid are lower since part of the windings volume in the CFD grid is related to insulators.

The no-load losses of the core are assumed to be spatially constant.

3.2.4. Boundary conditions

As only a part of the air cooling loop is simulated we employ in- and outlet boundary conditions. The inlet air flow is estimated via the ventilator characteristics. The inlet velocity is 5 m/s, the inlet temperature 300 K. Adiabatic conditions are assumed at all computation domain boundaries, except the in- and outlets.

Radiant heat transfer is considered at all structural material surfaces.

3.2.5. Simulation results

A vector representation of the velocity and a plot of the vertical velocity component are given in the figure below. They show the location of in- and outlet boundaries, core, three LV and one HV windings, radiation cylinder, and horizontal flow barrier. In the windings the vertical velocity component is about 4 m/s. Recirculation regions exist at the side wall of the enclosure and on top of the core.

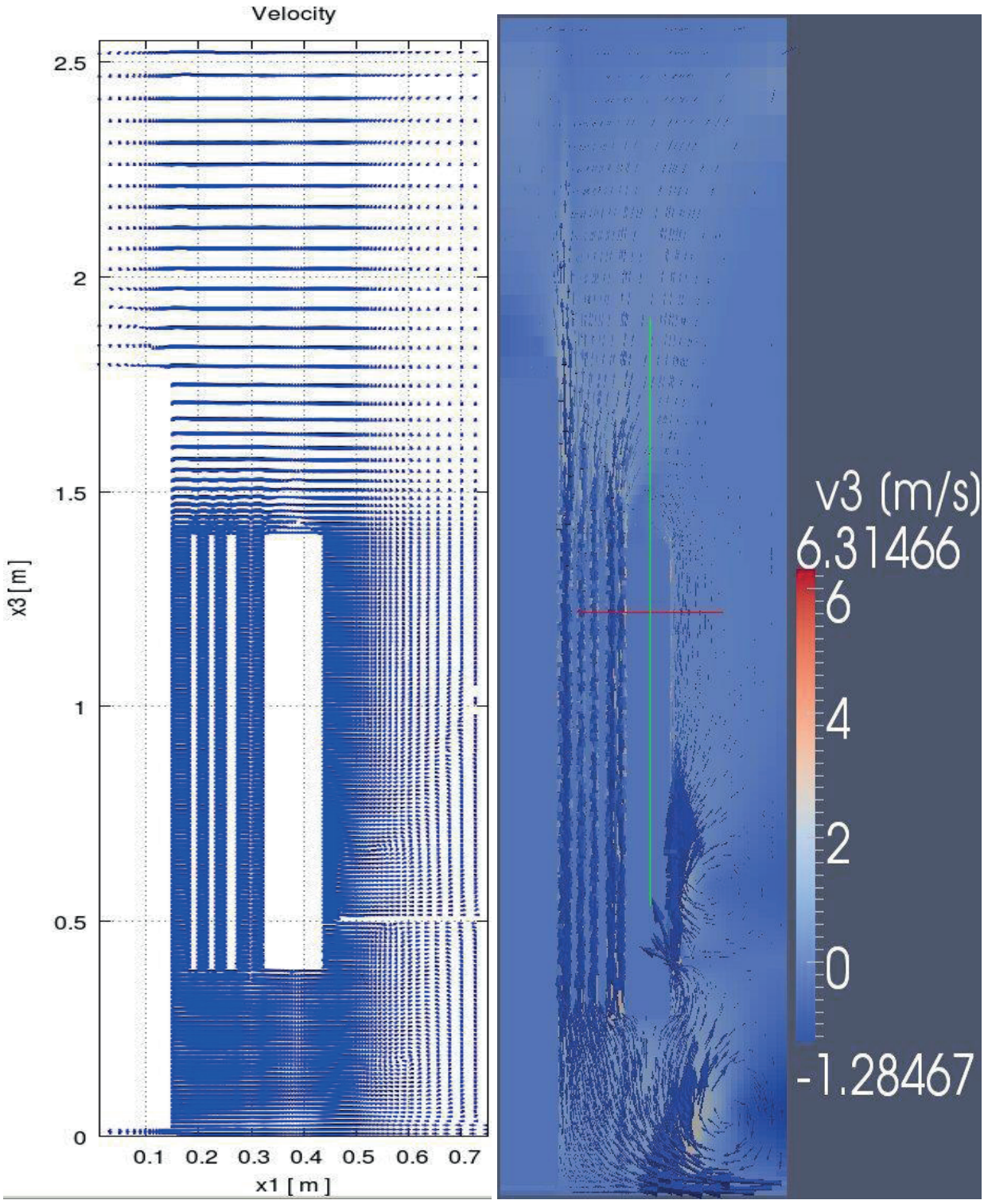

Figure 7 – Air velocity and vertical velocity component in cast resin transformer

A key result of the simulation is the temperature of air and structural materials shown in the figure below. The winding temperatures are related to local air velocity, radiant heat transfer, and spatial

variation of the power of the heat sources. In the HV windings lower temperatures correspond to the cast resin in the surroundings of the aluminium and the polyester. The 4 steps in the HV temperature are related to aluminium / polyester regions separated by cast resin. The figure also shows the upward convection of air heated up at the boundary layers adjacent to core, windings, and radiation cylinder.

As a result of the constant power density, in the radial direction there is a quadratic temperature profile in the core. However, the vertical temperature variation is much more pronounced.

Comparison of the left and right side of the figure shows that the radiation cylinder reduces the winding temperatures. This is most pronounced in the LV windings close to the radiation cylinder.

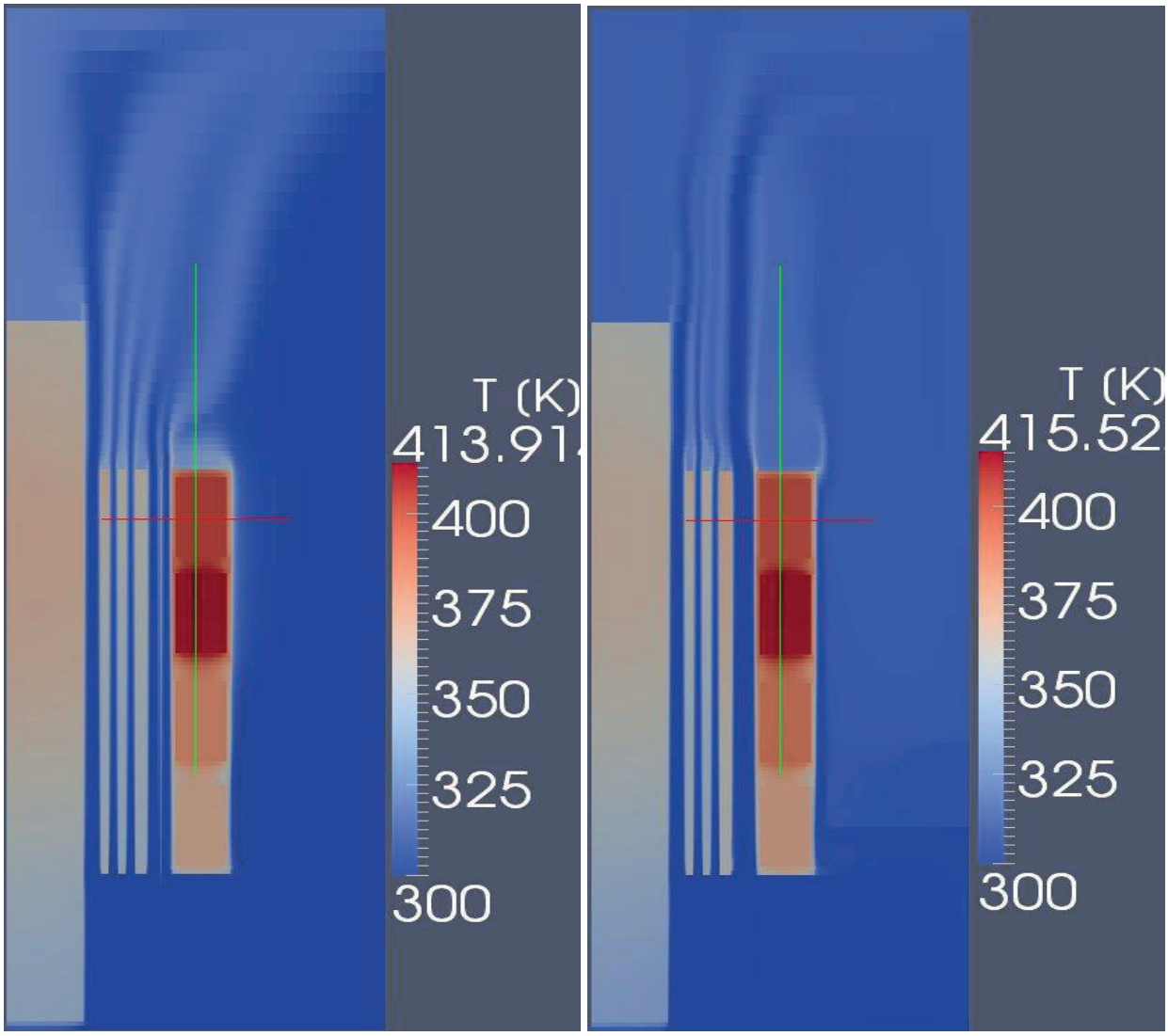

With radiation cylinder Without radiation cylinder

Figure 8 – Temperature of air, core, and windings in cast resin transformer

The investigated conditions in our analysis lead to maximum temperatures in the HV windings at the limit of class F material. The calculations can be used as a basis for design optimisation via a set of simulations with modification of various design parameters. For instance, the efficiency of the radiation cylinder between the LV and HV windings as a means of heat removal may be analysed via calculations with and without this cylinder.

4. CONCLUSION

The presented results indicate that UniFlow is a useful code for the thermal design of oil immersed and dry type transformers. It can be used to investigate advantages and shortcomings of design features and to perform design optimisation.

In addition to the results shown in this paper, also the pressure loss encountered in a device as a result of the fluid flow may be a major result of a simulation. This is demonstrated, e.g., in [10]. Other applications are related to detailed analyses on segments of disc windings with respect to, e.g., modelling of material compositions, width of oil channels, etc.. Another field of application are oil flows in cores. Moreover, combined oil and air flows are analysed in the context of fin type distribution transformers. This is aimed at, e.g., optimisation of the thermal efficiency of the fins. Furthermore, combined oil and air flows in radiators are investigated.

The calculated integral results of UniFlow, e.g., temperature differences between mid of windings and mid of oil channel, are similar to those calculated by correlation based methods. However, the spatial detail resolution of the results is superior.

REFERENCES

[1] Torriano, F., Chaaban, M., Picher, P., “Numerical study of parameters affecting the temperature distribution in a disc-type transformer winding”, Applied Thermal Engineering, 30, pp. 2034-2044, 2010

[2] Smolka, J., Nowak, A. J., ”Experimental validation of the coupled fluid flow, heat transfer and electromagnetic numerical model of the medium power dry-type electrical transformer”, Int. J. Thermal Sciences, 47, pp. 1393-1410, 2008

[3] Landau, L. D., Lifshitz, E. M., “Course of theoretical physics, vol. 6 : Fluid mechanics”, Pergamon Press, Oxford, UK, 1989

[4] Baehr, H. D., Stephan, K., "Heat and mass transfer“, Springer-Verlag, Berlin, 2006

[5] Ferziger, J. H., Peric, M., "Computational methods for fluid dynamics“, Springer-Verlag, Berlin, 1999

[6] van Doormal, J. P., Raithby, G. D., "Enhancements of the SIMPLE method for predicting incompressible flows“, Numer. Heat Transfer, 7, pp. 147-163, 1984

[7] Issa, R. I., "Solution of implicitly discretized fluid flow equations by operator splitting“, J. Comp. Phys., 62, pp. 40-65, 1986

[8] Trottenberg, U., Oosterlee, C. W., Schüller, A., "Multigrid“, Academic Press, New York, ISBN 012701070X, 2001

[9] Notay, Y., "An aggregation-based algebraic multigrid method“, Electronic Transactions on Numerical Analysis, 37, pp. 123-146, Kent State University, ISSN 1068-9613, 2010

[10] Tenbohlen, S., Weinläder, A., Wittmaack, R., "Prediction of the oil flow and temperature distribution in power transformers by CFD“, CIGRE Session 2010, Report A2-301, Paris, 2010

[11] Schlichting, H., “Boundary-layer theory”, McGraw-Hill, New York, USA, 1979